applied sciences

Article

Estimation of the Noise Source Level of a Commercial Ship Using On-Board Pressure Sensors

Hongseok Jeong [1], Jeung-Hoon Lee [2], Yong-Hyun Kim [2] and Hanshin Seol [1,*]

[1] Advanced Ship Reserach Division, Korea Research Institute of Ships and Ocean Engineering, Daejeon 34103, Korea; hsj@kriso.re.kr
[2] School of Mechanical Engineering, Changwon National University, Uichang-gu, Changwon 51140, Korea; jhoonlee@changwon.ac.kr (J.-H.L.); tw3315@gmail.com (Y.-H.K.)
* Correspondence: seol@kriso.re.kr; Tel.: +82-42-866-3468

Abstract: The dominant underwater noise source of a ship is known to be propeller cavitation. Recently, attempts have been made to quantify the source strength using on-board pressure sensors near the propeller, as this has advantages over conventional noise measurement. In this study, a beamforming method was used to estimate the source strength of a cavitating propeller. The method was validated against a model-scale measurement in a cavitation tunnel, which showed good agreement between the measured and estimated source levels. The method was also applied to a full-scale measurement, in which the source level was measured using an external hydrophone array. The estimated source level using the hull pressure sensors showed good agreement with the measured one above 400 Hz, which shows potential for noise monitoring using on-board sensors. A parametric study was carried out to check the practicality of the method. From the results, it was shown that a sufficient recording time is required to obtain a consistent level at high frequencies. Changing the frequency resolution had little effect on the result, as long as enough data were provided for the one-third octave band conversion. The number of sensors affected the mid- to low-frequency data.

Keywords: propeller cavitation; hull pressure; noise monitoring; underwater radiated noise

Citation: Jeong, H.; Lee, J.-H.; Kim, Y.-H.; Seol, H. Estimation of the Noise Source Level of a Commercial Ship Using On-Board Pressure Sensors. *Appl. Sci.* **2021**, *11*, 1243. https://doi.org/10.3390/app11031243

Academic Editor: Tomasz Figlus
Received: 22 December 2020
Accepted: 26 January 2021
Published: 29 January 2021

1. Introduction

The increase in commercial shipping has led to the development of ships with higher speeds and higher capacities, and the ambient noise of the sea has increased as a result [1,2]. Now, the noise pollution from commercial ships is considered to be one of the major issues in the ocean environment [3,4], and the International Maritime Organization (IMO) has set guidelines to mitigate it. In response to this, various research projects have been carried out, especially in Europe, to identify the radiated noise level as well as to reduce it.

It is well known that the dominant underwater noise source of commercial ships is propeller cavitation. Due to its impulsive characteristics, the cavitation affects the tonal noise at blade-passing frequencies (BPFs) as well as the broadband noise. The radiated noise can be measured by a procedure based on ISO 17208-1 [5], which exploits an external noise measurement system located away from the target vessel [6–8]. However, this has several disadvantages in cost and time, and the measured noise is affected by the sea state. In addition, the test cannot be conducted for all operating conditions, so only a limited set of data can be obtained. More importantly, the noise level cannot be monitored after the measurement, which makes it difficult to know how much the noise is radiated during actual operations. This may not be a problem for noise monitoring close to shore, but the system can only cover a limited area [9–12].

In terms of experimental approaches, model-scale tests have helped greatly in understanding cavitation behavior and radiated noise. Many studies have been carried out to predict the full-scale noise spectrum based on the scaling law recommended by International Towing Tank Conference [13]. Although the scaling exponents may be different from the recommended values, it was shown that the model-scale measurements could give reasonable estimations of the radiated noise at full scale with the scaling law [14–17]. Still, there is room for improvement in the accuracy of these tests. This includes the viscous scaling effects, wake at the propeller plane, nucleus distribution, etc. In addition, the inconsistency in the results between different test facilities is still in question [18].

Numerical methods could also be used to predict the radiated noise as well as to analyze the noise-generating mechanism. These include the boundary element method (BEM) [19], potential flow theory, or computational fluid dynamics (CFD) with an acoustic analogy [20–23]. Although these are being rapidly developed, gaps still exist between measurements and predictions.

As model-scale measurements and numerical predictions can only be used for certain conditions, the need to make use of on-board sensors for noise monitoring is inevitable. An early attempt was made by Ten Wolde and De Brujin [24], who measured the source strength of a ship propeller using the principle of reciprocity. They developed a method using the transfer function between the cavitating propeller and the sound and vibration inside a ship. The method showed consistent volume acceleration at the propeller, which was calculated using the transfer functions from various locations where the other noise sources were not dominant.

The fact that the cavitation and the hull pressure fluctuation are related led to the development of source strength estimation methods using measurements of hull pressure. For example, Wijngaarden [25] formulated an inversion equation for estimating the source strength distribution using the BEM. An example of a single screw ship case was shown, in which a single monopole source was assumed. An initial source location was defined and the discrepancy between the measured and calculated hull pressures was calculated. By changing the source location, the point where the discrepancy was at its minimum was found. A similar approach can be found in the study by Lee et al. [26]. Differently from [25], the boundary element integral equation was not modified, and an optimization technique was employed to find the locations and the strengths of the sources. Similar concepts can be found in the time difference of arrival (TDOA) method [27] or compressive sensing (CS) method [28,29]. These have advantages over the inversion method, as they do not require prior knowledge of the acoustic pressure field. However, iterative calculations and optimization techniques are needed for the TDOA method and the CS method, respectively.

For these reasons, it seems obvious that on-board sensors need to be used to constantly monitor the underwater radiated noise. In addition, as the computation time is an important factor, the estimation method should be simplified to some extent. In this regard, Turkmen et al. [30] tried to estimate the underwater radiated noise from a research vessel using on-board sensors. With an empirical formula, comparisons between the measured hull pressure and radiated noise level were made for blade-passing frequency components. Foeth and Bosschers [31] presented a nearfield beamforming method with minimum-variation distortionless response (MVDR) to localize the incipient cavitation. The method was validated in a model-scale test, and the results at full scale showed good agreement between the measured and estimated values from 4 to 16 kHz. This method has an advantage in the computational cost by assuming a single monopole source. This made the estimation process into a minimization problem that can simply be calculated in the region of interest.

In this study, the beamforming method presented in [31] was employed without the MVDR. Although it is unlikely that the propeller of a commercial ship exhibits incipient cavitation at operating conditions, a single monopole source was assumed for simplicity. The method is briefly introduced and formulated in Section 2. For validation of the method, a model-scale measurement was carried out with a hydrophone sensor array at the hull surface above the propeller. Using a hydrophone at the bottom of the tunnel and a source of known transmitting voltage response (TVR), the source level was measured and compared with the estimated one. For the same ship, a full-scale trial was conducted with flush-mounted pressure transducers installed on the hull surface. The underwater radiated noise was measured using a buoy-type hydrophone array with three self-recording hydrophones, and the results were converted into the source level. Using the measured hull pressures, the source level was estimated and compared with the measured one. A parametric study was conducted to check the sensitivity of the measurement variables to the result.

2. Method and Validation

2.1. Methodology

A simplified beamforming-based source-level estimation method [31] was used in the current study. It was assumed that, at a given frequency, the noise source can be represented by a single monopole source in a quiescent fluid. With M sensors at the hull, the measured sound pressure at the m-th sensor (y_m) can be calculated as

$$y_m = \frac{e^{-\mathrm{i}kr_m}}{r_m} s + e, \tag{1}$$

where r_m is the distance between the source and the receiver, $k = 2\pi f / c$ is the wavenumber, s is the source strength of the monopole, and e is unwanted noise. As Equation (1) is defined in the frequency domain, y_m is the pressure converted from time-series data using the Fourier transform. It should be noted that the use of the free-space Green function could lead to overprediction of the source level at low frequencies, as the measured signal would be greater due to solid boundaries around the source.

For M on-board sensors, Equation (1) can be written as

$$\mathbf{y} = s\mathbf{a} + \mathbf{e}, \tag{2}$$

where

$$\mathbf{y} = \begin{bmatrix} y_1 \\ y_2 \\ \vdots \\ y_M \end{bmatrix}, \quad \mathbf{a} = \begin{bmatrix} \frac{e^{-\mathrm{i}kr_1}}{r_1} \\ \frac{e^{-\mathrm{i}kr_2}}{r_2} \\ \vdots \\ \frac{e^{-\mathrm{i}kr_M}}{r_M} \end{bmatrix}, \quad \mathbf{e} = \begin{bmatrix} e_1 \\ e_2 \\ \vdots \\ e_M \end{bmatrix}. \tag{3}$$

In the general beamforming method, a scan vector would be made for a virtual sound source in the region of interest to calculate the maximum beamforming power with the measurement vector $\mathbf{y}$. In this case, however, the source strength is not given. To resolve this, an assumed source strength E was introduced; the problem is thus changed into a minimization problem and is written as

$$\min cost = \frac{1}{M^2} \|\mathbf{Y} - E^2\mathbf{A}\|_F^2. \tag{4}$$

Here, $\|\cdot\|_F$ is the Frobenius norm, $\mathbf{Y} = (\mathbf{y}\mathbf{y}^{\mathrm{H}})$ is the correlation matrix of the measurement vector, and $\mathbf{A} = (\mathbf{a}\mathbf{a}^{\mathrm{H}})$ is the correlation matrix of the propagation vector. The superscript 'H' indicates the conjugate transposition. The right-hand side of Equation (4) without M^2 can be rewritten as

$$\|\mathbf{Y} - E^2\mathbf{A}\|_F^2 = \mathrm{tr}(\mathbf{Y}\mathbf{Y}^{\mathrm{H}}) - E^2\mathrm{tr}(\mathbf{Y}^{\mathrm{H}}\mathbf{A}) - E^2\mathrm{tr}(\mathbf{Y}\mathbf{A}^{\mathrm{H}}) + E^4\mathrm{tr}(\mathbf{A}\mathbf{A}^{\mathrm{H}}). \tag{5}$$

Here, the operator 'tr' is the trace of a matrix. Taking the derivative with respect to E and letting the derivative be zero yields

$$\frac{\partial\|\mathbf{Y} - E^2\mathbf{A}\|_F^2}{\partial E} = -2E\mathrm{tr}(\mathbf{Y}^{\mathrm{H}}\mathbf{A}) - 2E\mathrm{tr}(\mathbf{Y}\mathbf{A}^{\mathrm{H}}) + 4E^3\mathrm{tr}(\mathbf{A}\mathbf{A}^{\mathrm{H}}) = 0. \tag{6}$$

The virtual source strength E can be obtained by solving Equation (6), i.e.,:

$$E = \sqrt{\frac{\mathrm{tr}(\mathbf{A}^{\mathrm{H}}\mathbf{Y})}{\mathrm{tr}(\mathbf{A}^{\mathrm{H}}\mathbf{A})}}. \tag{7}$$

Substituting Equation (7) into Equation (5) yields

$$\|\mathbf{Y} - E^2\mathbf{A}\|_F^2 = \mathrm{tr}(\mathbf{Y}^{\mathrm{H}}\mathbf{Y}) - \frac{\mathrm{tr}(\mathbf{A}^{\mathrm{H}}\mathbf{Y})^2}{\mathrm{tr}(\mathbf{A}^{\mathrm{H}}\mathbf{A})}. \tag{8}$$

As the first term on the right-hand side of Equation (8) depends only on the measurement, the second term should be maximized to minimize the cost function. In other words, the minimization problem can be seen as a maximization problem, which can be expressed as

$$\max cost = \frac{\mathrm{tr}(\mathbf{A}^{\mathrm{H}}\mathbf{Y})^2}{\mathrm{tr}(\mathbf{A}^{\mathrm{H}}\mathbf{A})}. \tag{9}$$

For simplicity of notation, the cost function in Equation (9) is replaced with α in the rest of the paper.

The meaning of Equation (8) can be explained by the following example. Assume that a single monopole source is placed at $\mathbf{q}$ in a two-dimensional space, which is shown in Figure 1. The sound pressure is measured by an array consisting of two sensors. A virtual source region is set with two points, one of which is the true source location. At frequency f, the measured signals at the array are y_1 and y_2. The propagation vectors can be calculated using Equation (3), which are expressed as $\mathbf{a}$ and $\mathbf{a}'$.

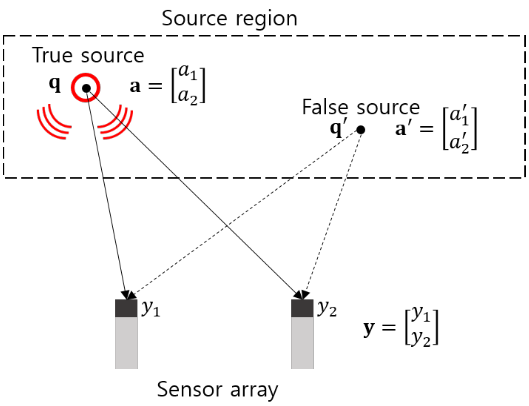

Figure 1. Example of the beamforming problem.

For the true source point, Equation (1) reduces to

$$\mathbf{y} = s\mathbf{a}. \tag{10}$$

Accordingly, the relation between the matrices $\mathbf{Y}$ and $\mathbf{A}$ can be expressed as

$$\mathbf{Y} = |s|^2\mathbf{A}. \tag{11}$$

Substituting Equation (11) into Equation (8) yields

$$\|\mathbf{Y} - E^2\mathbf{A}\|_F^2 = |s|^4\mathrm{tr}(\mathbf{A}^{\mathrm{H}}\mathbf{A}) - \frac{|s|^4\mathrm{tr}(\mathbf{A}^{\mathrm{H}}\mathbf{A})^2}{\mathrm{tr}(\mathbf{A}^{\mathrm{H}}\mathbf{A})} = 0. \tag{12}$$

As the left-hand side of Equation (8) is a non-negative value, Equation (12) shows that for the true source location, the cost function is minimized. For the false source location, this can be written as

$$\|\mathbf{Y} - E^2\mathbf{A}\|_F^2 = \left(|y_1|^2 + |y_2|^2\right)^2 - \frac{\left(|a_1'|^2|y_1|^2 + a_1'\overline{a_2'}y_2\overline{y_1} + a_2'\overline{a_1'}y_2\overline{y_1} + |a_2'|^2|y_2|^2\right)^2}{\left(|a_1'|^2 + |a_2'|^2\right)^2}. \quad (13)$$

It can be seen that the second term of the right-hand side of Equation (13) depends on the propagation vector $\mathbf{a}'$, and thus, the cost function is always greater than zero.

In the actual application, the cost function is calculated at each point in the source region and the point where the cost function is minimum is determined. The corresponding source strength E is then calculated from Equation (7). The whole procedure is summarized in Figure 2. It should be noted that the method works well when the actual cavitation noise sources are concentrated within a single region because a single monopole source at a single point is assumed at each frequency.

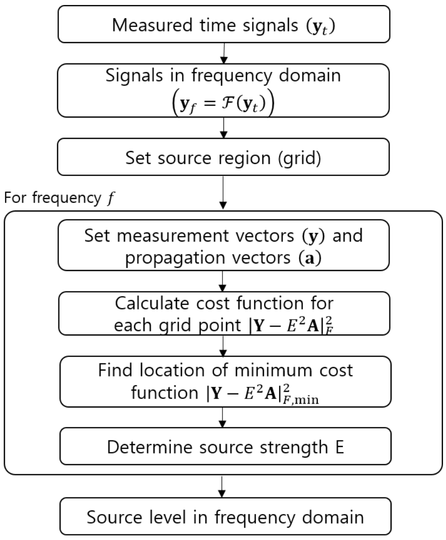

Figure 2. Procedure of the source-level estimation.

2.2. Validation of the Method

To check the validity of the estimation method, a model-scale measurement was conducted in the Large Cavitation Tunnel (LCT) at the Korea Research Institute of Ships and Ocean Engineering (KRISO). Figure 3 shows a schematic view of the tunnel. The overall dimensions of the tunnel are 60 × 22.5 × 6.5 m^3, and those of the test section are 12.5 × 2.8 × 1.8 m^3. A model ship and propeller with a scale ratio of 25.6 were installed in the test section, as shown in Figure 4.

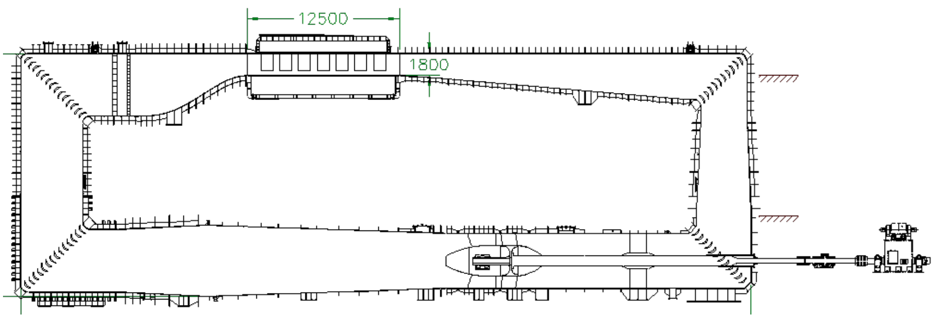

Figure 3. Schematic view of the Large Cavitation Tunnel (LCT) at the Korea Research Institute of Ships and Ocean Engineering (KRISO).

Figure 4. Model ship installed in the LCT.

A set of B&K type 8103 miniature hydrophones were installed at the hull above the propeller plane for the estimation of source strength. The position and the coordinates of the hydrophones on the hull are shown in Figure 5 and Table 1, respectively. As the hydrophones were not flush-mounted, they were expected to be affected by flow noise. This would be small, however, unless cavitation were to occur directly around the hydrophones. All the hydrophone sensors were connected to a B&K type 2692-A charge amplifier and B&K type 3052 data acquisition system, which provided a sampling frequency of up to 204.8 kHz.

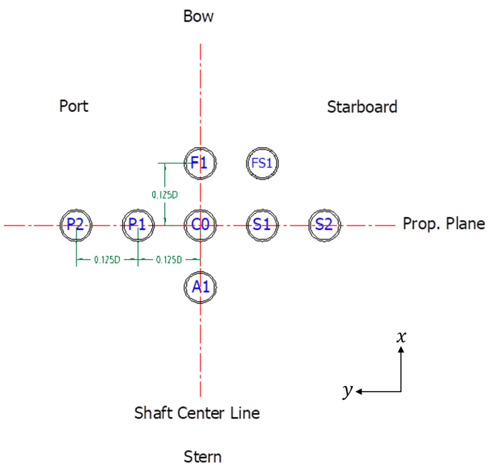

Figure 5. Position of the hydrophones at the hull surface (projected).

Table 1. Coordinates of the hydrophones at the hull surface (projected).

Position	x (mm)	y (mm)
P2	0	62.5
P1	0	31.25
C0	0	0
S1	0	−31.25
S2	0	−62.5
F1	31.25	0
A1	−31.25	0
FS1	31.25	−31.25

To obtain the source level from the measurement, a B&K type 8105 hydrophone was used in an acoustic window at the bottom of the tunnel. The test procedure was as follows. Firstly, the background noise was measured without the propeller in the presence of the flow. Secondly, the propeller noise was measured at the test condition. The background noise correction was then applied to obtain valid data (SPL_m). To calculate the source level, it was necessary to measure the transfer function between the source and the receiver. This could be done by replacing the propeller with a sound source of known properties and measuring the source and receiver signals simultaneously. Note that in the transfer function measurement, the flow speed was set to be zero. In this study, an ITC-1032 transducer was used, for which the setup is shown in Figure 6. The transfer function measurement is usually carried out for different source positions along the propeller disk in the circumferential direction. However, only the center position was considered in this study, as the difference was negligible. To obtain more accurate results, one may look at the cavitation pattern to identify possible source locations.

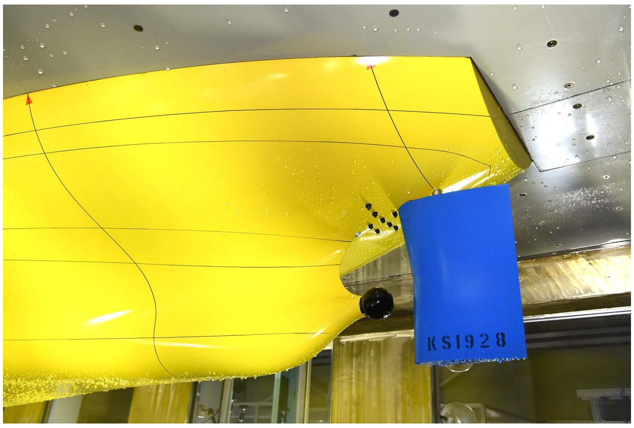

Figure 6. Setup for transfer function measurement.

The source level in model-scale measurements can be obtained as follows:

$$SL_m = SPL_m + TVR - TF \quad \text{(dB)}, \tag{14}$$

where SL_m is the source level at the model scale, TVR is the transmitting voltage response of the transducer in free field, and TF is the transfer function. The transmitting voltage response was provided in the transducer data sheet, as shown in Figure 7. The transfer function between the source and the hydrophone in the tunnel was measured, and the result is shown in Figure 8. Using these two graphs, the source level in free field can be obtained for a given operating condition.

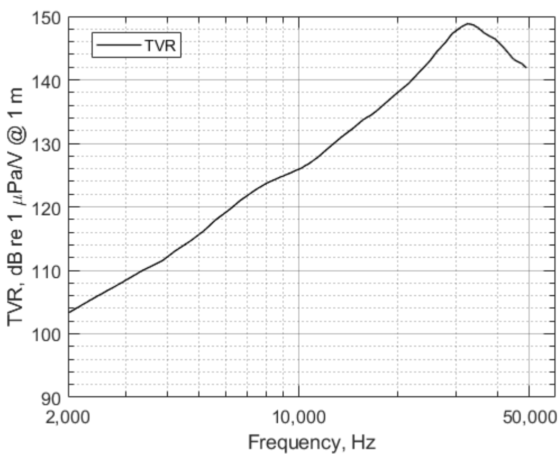

Figure 7. Transmitting voltage response of the ITC-1032 (from product data sheet).

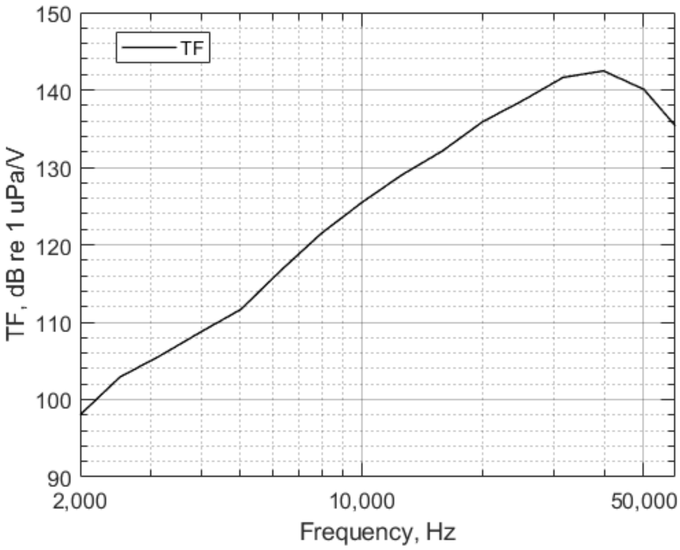

Figure 8. Measured transfer function between the source and sensor in the tunnel.

Three operating conditions were considered in the measurement, as shown in Table 2. Here, the cavitation number $\sigma_{n,0.7R}$ is defined as

$$\sigma_{n,0.7R} = \frac{p_c - \rho g h_{0.7R} - p_v}{\frac{1}{2}\rho n^2 D^2}, \tag{15}$$

where p_c is the pressure at the center of the tunnel, ρ is the density of the fluid, g is the gravitational acceleration, $h_{0.7R}$ is the height that is defined from the center of the tunnel to the $0.7R$ upward position, p_v is the vapor pressure, n is the rotational speed of the propeller, and D is the diameter of the propeller. The flow speed V was set to be 7 m/s, and the tunnel pressure was controlled to tune the cavitation number. The water temperature was 16.3 °C. Each run was recorded for 60 s with a sampling frequency of 204.8 kHz. The data were post-processed using MATLAB to obtain the power spectral density (PSD).

Table 2. Model test conditions.

Condition	V (m/s)	$\sigma_{n,0.7R}$	n (rps)
C1	7.0	3.06	44.04
C2	7.0	2.82	44.16
C3	7.0	2.61	44.30

Figure 9 shows a comparison between the measured signals in operating condition $C1$ and the background noise. For the hull pressure sensors, the result at the "C0" position were plotted. From the graphs, it can be seen that the result above 200 Hz can be used without correction. However, the TVR of ITC-1032 is uncalibrated at frequencies below 2 kHz. Therefore, the result at frequencies above 2 kHz is valid. It is also seen that the shaft rate components and the blade rate components have a strong effect on the spectrum below 2 kHz. These components may not be estimated well, even if the transducer covers this frequency range, as monopole-like sound propagation is assumed. The cavitation noise is dominant above 2 kHz, where a smooth curve is seen. The peaks around 20 kHz are the singing noise caused by structural resonances at the trailing edge of the propeller blades.

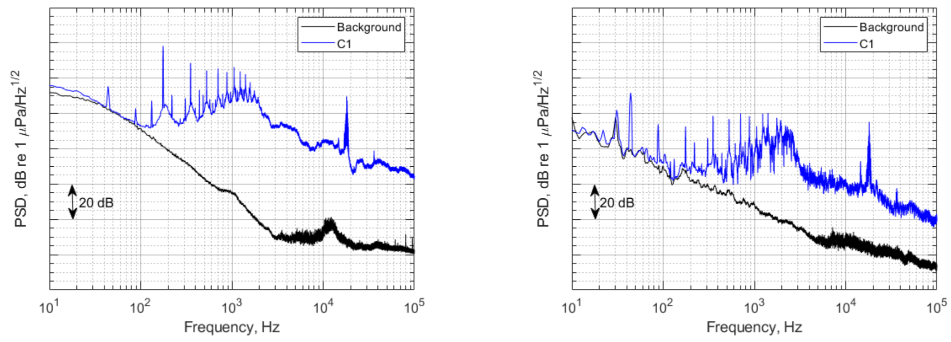

(**a**) (**b**)

Figure 9. Comparison between the measured signal and background noise: (**a**) hull sensor and (**b**) sensor at the tunnel bottom.

To calculate the source level, a hexahedral source region was set around the propeller, which is shown in Figure 10. The ranges of y and z are defined symmetrically with respect to the propeller center, from $-0.6D$ to $0.6D$, where D is the propeller diameter. The range of x is defined from -0.1 to 0.1 m. The spacing was set to be 0.01 m in all directions.

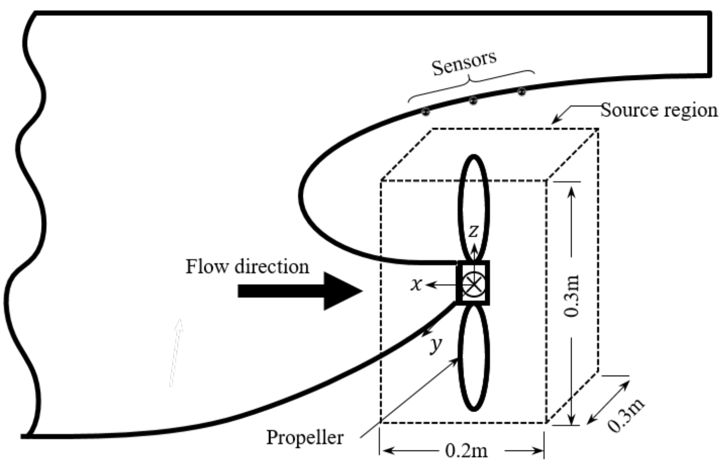

Figure 10. Assumed source region.

The sound pressure measured from the sensors at the hull was converted using the Fourier transform. For the source-level estimation, the frequency range was set from 1 to 100 kHz with a spacing of 32 Hz. For the grid points in the source region, α was calculated. Figure 11 shows the normalized values of α in the source region at 8 and 40 kHz, for example. A strong noise source is seen between the 12 o'clock position and 1 o'clock position viewed from the stern side. In addition, it can be seen that the source was located downstream close to the propeller. At 8 kHz, the source was located in one region, whereas two main source regions are seen at 40 kHz. For this reason, α is lower in the 40 kHz result.

For comparison, the cavitation pattern for condition C3 is shown in Figure 12. Note that the angle is defined at the 12 o'clock position viewed from the stern side in the clockwise direction. It can be seen that the cavitation occurs strongly on the starboard side, which is also found in Figure 11. Thus, it can be said that the method reasonably describes the noise source.

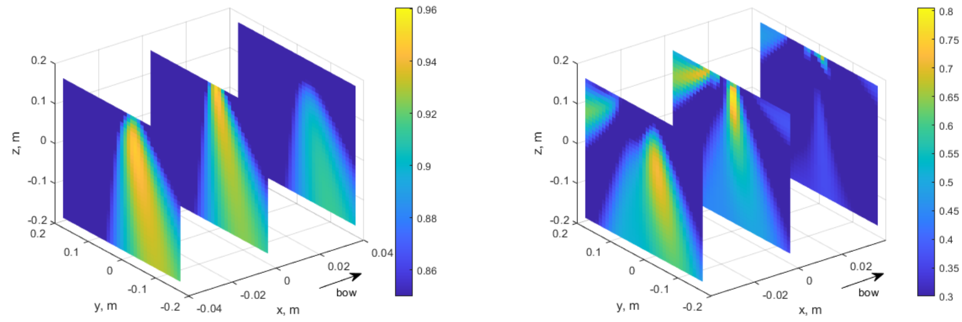

(**a**) (**b**)

Figure 11. Normalized α at (**a**) 8 kHz and (**b**) 40 kHz (condition *C*3).

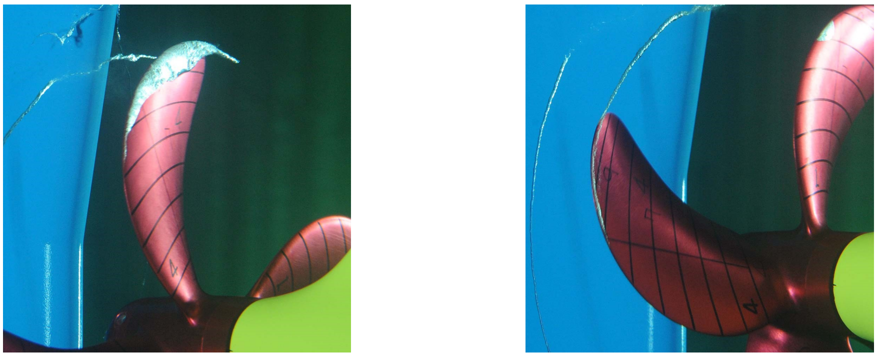

(**a**) (**b**)

Figure 12. Cavitation pattern at (**a**) 20° and (**b**) 80° (condition *C*3).

From the α map, the maximum value was found, and the corresponding source level was obtained. Having obtained the source level at all frequencies, the result was compared with the measured source level, which is shown in Figure 13 in terms of spectral density. Overall, the calculated source level agreed well with the measured one from 2 to 50 kHz. The differences below 2 kHz were due to the combination of the monopole assumption and the transducer characteristics. Above 50 kHz, the transfer function could not be applied, and thus, the predicted source level deviated from the measured one. From this, it can be said that the proposed method is valid.

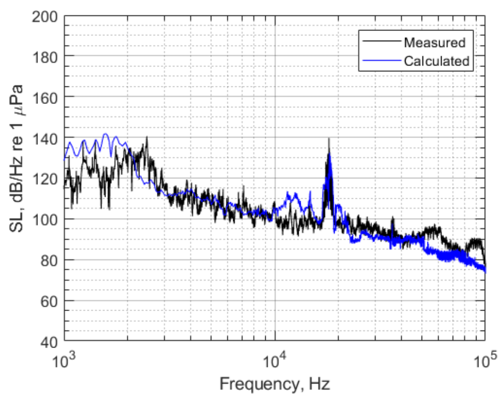

Figure 13. Comparison between measured and calculated source levels for condition *C*1.

Comparisons were also made for the other conditions. This is illustrated in Figure 14. The same conclusion can be drawn, with few differences in the results.

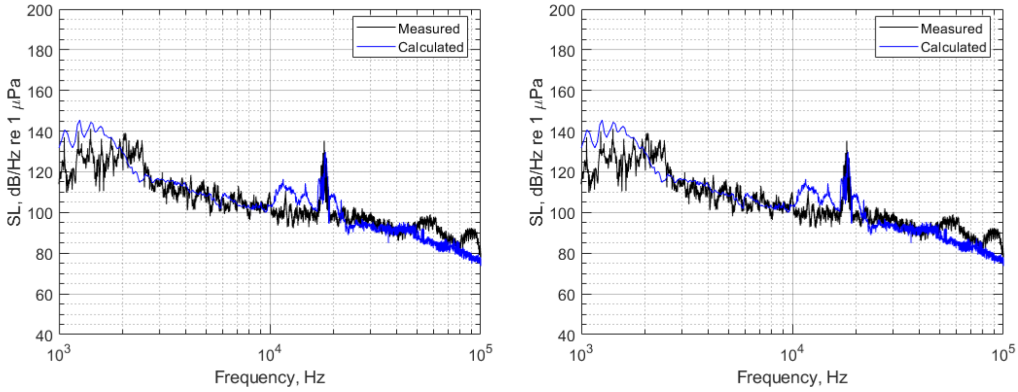

(**a**) (**b**)

Figure 14. Comparison between the measured and calculated source levels for conditions (**a**) *C*2 and (**b**) *C*3.

3. Source-Level Estimation at Full Scale

In this section, the source level of a full-scale ship was estimated with the presented method. A 50 k product carrier was selected as a target vessel, which was the model ship used in the validation test.

3.1. Underwater Radiated Noise (URN) Measurement

A full-scale URN measurement of the vessel of interest (see Figure 15) was carried out by the Korea Institute of Ocean Science and Technology (KIOST) in March 2014. The test site was in the South Sea of Korea (see Figure 16), in which the depth was around 105 m. Figure 16b shows the test course. "St.10" (or "St.9") is the start/end point of the measurement, and "St.5" (or "St.4") is the start/end point of the data acquisition. "St.8" is the closest point of approach (CPA), which is 300 m from "St.3". The distance from "St.8" to "St.5" (or "St.4") is 173 m, and that from "St.8" to "St.10" (or "St.9") is 692 m. These distances are nominal distances, as in the measurement, they kept changing due to wind, tide, current, and ship operation. Therefore, relative distances were recorded using GPS and were used for the source-level calculation.

To measure the underwater radiated noise, a buoy-type hydrophone array was deployed. A schematic view of the hydrophone array is shown in Figure 17. The array consisted of a surface buoy with GPS, three self-recording hydrophones with a depth sensor, sub-surface buoys, an acoustic release, and a weight (train wheel) at the bottom. A GPS sensor was installed in the target vessel to calculate the relative distance.

Figure 15. Target vessel.

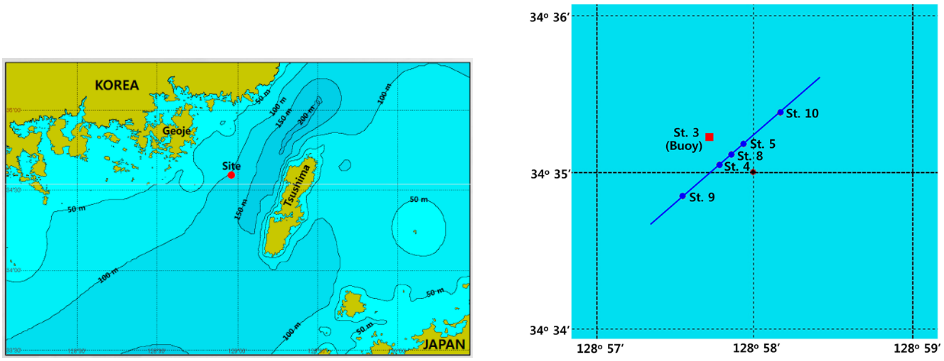

(**a**) (**b**)

Figure 16. Test site for underwater radiated noise (URN) measurement: (**a**) location and (**b**) test course.

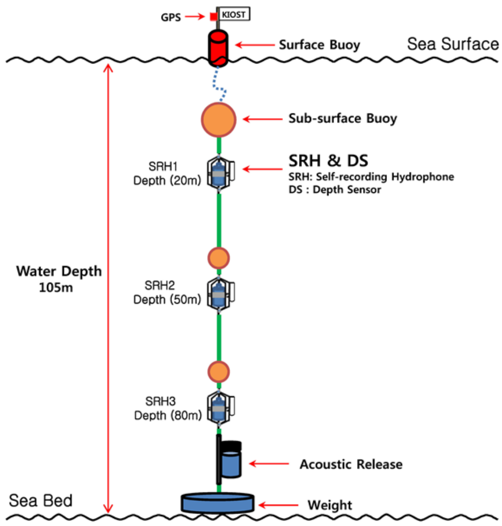

Figure 17. Schematic view of the URN measurement setup.

The test procedure was based on ISO 17208-1, although the test area was a shallow water. For each condition, the measurement was conducted for both sides of the ship, and the results were processed as follows. Firstly, for measured data (L_{p+n}) and background noise (L_n), an incoherent background noise correction was made. The rules for the correction were as follows:

- For $\Delta L \leq 3$ dB: data to be discarded;
- For 10 dB $\leq \Delta L \geq 3$ dB: $L_p' = 10\log_{10}\left[10^{L_{p+n}/10} - 10^{L_n/10}\right]$ (dB);
- For $\Delta L \geq 10$ dB: no corrections.

Here, $\Delta L \left(= L_{p+n} - L_n\right)$ is the difference between the measured signal and the background noise in decibels. After the background noise correction, a distance correction was made using a monopole sound source assumption. This can be written as

$$L(r)_{RN,i} = L_p' + 20\log_{10} d_T/d_{ref} \quad \text{(dB)}, \tag{16}$$

where $L(r)_{RN,i}$ is the corrected sound source level at the i-th hydrophone in the r-th run, d_T is the distance between the hydrophone and the acoustic center of the ship at the closest point of approach (CPA), and d_{ref} is the reference distance (1 m). Here, the CPA is defined as the point at which the distance between the hydrophone array and the target vessel is the shortest.

A spatially averaged value of each run can be calculated as

$$L(r)_{RN} = 10\log_{10}\left[\frac{\sum_{i=1}^{3} 10^{L(r)_{RN,i}/10}}{3}\right]. \tag{17}$$

The spatially averaged source level is again averaged for all runs, i.e.,

$$L_{RN} = 10\log_{10}\left[\frac{\sum_{r=1}^{k} 10^{L(r)_{RN}/10}}{k}\right], \tag{18}$$

where k represents the number of runs for each condition. The same operating conditions were considered as in the model-scale measurement. The shaft RPM values for the conditions were 95, 99, and 103, respectively. For each condition, the measurement was carried out twice ($k = 2$). The radiated noise was measured with a sampling frequency of 60 kHz, and the result was processed to the source level in one-third octave bands.

3.2. Hull Pressure Measurement

For the hull pressure measurement, several holes were made at the hull surface above the propeller [14,32]. Figure 18 shows a 3D model of the holes in the hull. It can be seen that the sensor holes were not exactly on the line of propeller plane or on the centerline. This was due to the presence of beam structures, which are seen in Figure 19 for the sensors at $C0$, $S1$, and $S2$. The coordinates of the sensors are listed in Table 3. Note that the origin (0,0) is the point where the centerline and the propeller plane cross.

(**a**) (**b**)

Figure 18. Positions of the pressure sensors (bottom view): (**a**) overall and (**b**) relative to the propeller.

Figure 19. Pressure sensors at $C0$, $S1$, and $S2$ installed on the line of the propeller plane.

Table 3. Positions of the pressure sensors; (0,0) = center of the propeller.

Position	x(mm)	y (mm)
P2	−78	1400
P1	−78	600
C0	−78	−200
S1	−78	−1000
S2	−78	−1800
F1	848	−200
F2	1648	−200

For the measurement, Kulite XTM 190 pressure transducers with an HBM amplifier and a B&K data acquisition system were used. No corrections were made for these signals, as the measured signal was more than 10 dB greater than the background noise at all frequencies.

Differently from the URN measurement, the hull pressure measurement does not need an exact data window (between “St.4” and “St.5” in Figure 16b) unless the pressures are to be synchronized with the URN. Therefore, if the operating condition does not change, the result is expected to be consistent. In the measurement, the time window of data recording was set to be one minute, during which the operating condition remained unchanged. Although this was within the data acquisition region, the hull pressures were not exactly synchronized with the URN data.

3.3. Results and Discussion

Using the simple beamforming method, the source level was estimated for each run, and the results were averaged. The source region was set as

$$\begin{aligned} -2\,\mathrm{m} &\leq x \leq 2\,\mathrm{m} \\ -0.6D &\leq y \leq 0.6D \\ -0.6D &\leq z \leq 0.6D, \end{aligned} \tag{19}$$

where D is the propeller diameter. The spacing was 0.1 m in all directions and the frequency resolution was 4 Hz. The estimated source level was compared with the measured source level in one-third octave bands. The results for operating condition $C1$ are plotted in Figure 20. It is seen that at low frequencies below 100 Hz, the estimated source level is about 20 dB larger than the measured one. The reasons for this discrepancy would mainly be the distance between the propeller (source) and the sensors (receiver), which was about 5 m. The corresponding wavelength from the relation $\lambda/2 = r$ is 10 m and the frequency is $f_{\text{min}} = c/\lambda$ = 150 Hz. This is the case when the source is placed at the center of the propeller. In reality, the source location varies within the propeller disc, depending on the cavitation pattern. In most cases, cavitation occurs when the propeller passes the upper part of the propeller plane, so that f_{min} increases as the distance becomes shorter. The shortest distance corresponds to the 400 Hz band; hence, inaccuracy still exists between 150 and 400 Hz. Above this frequency, the agreement between the results is good, showing discrepancies within 6 dB.

The Lloyd mirror effect due to the presence of free surface and the reflection from the sea bottom could also have played a role at low frequencies. As an example, the transmission loss (TL) due to the free-surface effect at hydrophone position (50 m depth) was calculated and plotted in Figure 21. A TL of less than 10 dB is seen below 100 Hz, which suggests that the measured URN could increase if this effect were to be considered. The reflection, however, is thought to be less significant, as inclusion of the reflection would have increased the measured URN. If the data measured from the deepest hydrophone (80 m depth) were considered, the measured URN would be less than the plotted value [7].

As the data measured from individual hydrophones were not provided, comparisons could not be made.

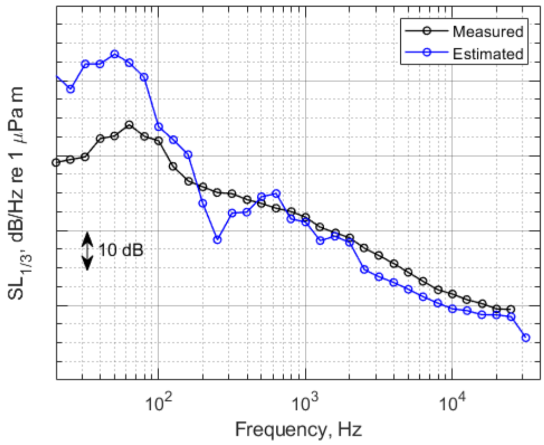

Figure 20. Comparison of measured and estimated source levels for condition *C*1.

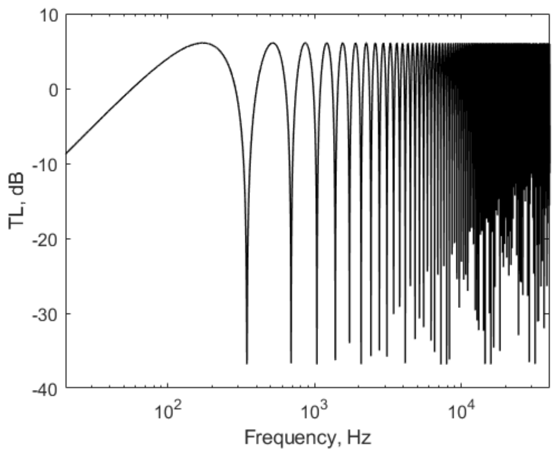

Figure 21. Calculated transmission loss at the hydrophone position (50 m depth).

The results for conditions *C*2 and *C*3 are also plotted in Figure 22. The agreement is better at high frequencies, as the signal-to-noise ratio increases.

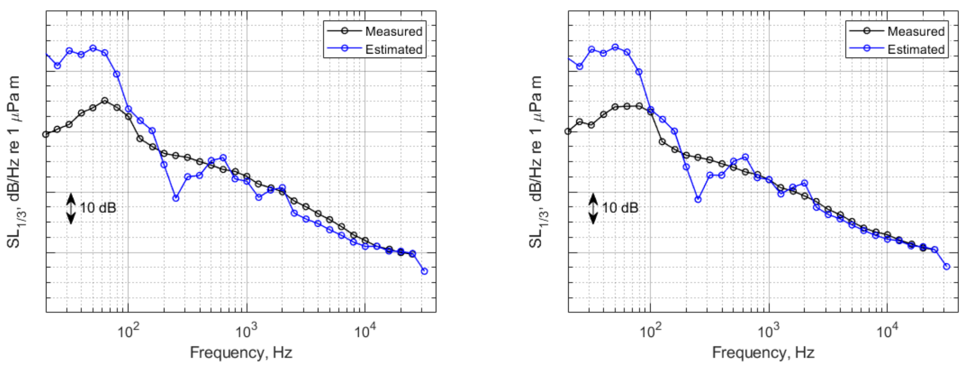

(**a**) (**b**)

Figure 22. Comparison of measured and estimated source levels for different conditions: (**a**) C2 and (**b**) *C*3.

For a quantitative comparison, the differences between the measured and estimated source levels are listed in Table 4 for different octave band center frequencies. As seen in Figures 20 and 22, the differences are within 6 dB above 500 Hz.

Table 4. Differences between measured and estimated source levels.

Octave Band Center Frequency, Hz	$SL_{estimated}$-$SL_{measured}$, dB $C1$	$C2$	$C3$
31.5	24.8	24.4	25.1
63	16.6	15.8	17.9
125	7.1	6.0	7.4
250	−12.6	−14.1	−13.9
500	1.8	1.6	2.0
1000	−1.3	−1.6	0.1
2000	−1.2	1.4	4.3
4000	−5.0	−3.3	−1.3
8000	−3.5	−2.3	−1.1
16,000	−2.9	−0.6	−0.6

As the method was developed for noise monitoring, the source level should be obtained for a short recording time with a limited number of sensors. In addition, the number of frequencies for data processing should also be minimized in order to reduce the computation time. A sensitivity analysis was conducted to check these aspects for condition $C1$. The parameters are listed in Table 5.

Table 5. Parameters for the sensitivity analysis.

Parameter	Range
Recording time (Δt), s	60, 10, 2
Frequency resolution (Δf), Hz	4, 16, 64
Number of sensors	7, 5, 3

The source levels for two different recording times (10 s and 2 s) are shown in Figure 23. As the total measurement duration was 60 s, three different time ranges were chosen to check the consistency of the results. It can be seen that the results did not change much when Δt = 10 s. When Δt was set to be 2 s, the results above 8 kHz became slightly different, showing a difference of up to 6 dB. Compared to the "10 s" case, the source level was overestimated compared to that in Figure 20. This could be due to the randomness of the propeller cavitation, which could not be captured entirely by a short-term measurement. Apart from that, the agreement with the measured data is good in terms of trend and level.

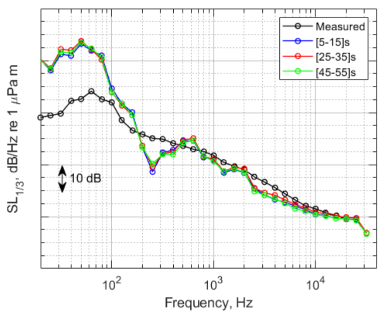

(**a**)

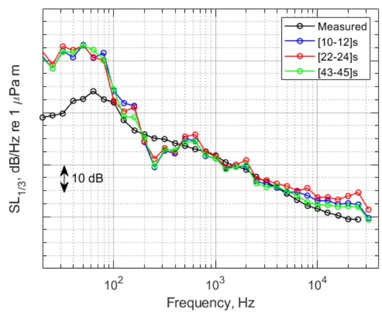

(**b**)

Figure 23. Comparison of the source levels estimated for different recording times: (**a**) 10 s and (**b**) 2 s.

The recording time may not be as important as the other parameters, provided that it guarantees a consistent result. The other two variables are, however, directly related to the computation time, and are thus very important in noise monitoring. For the variable ranges listed in Table 5, the corresponding results are plotted in Figure 24. For different frequency resolutions, three results showed very similar behaviors above 300 Hz. It should be noted that as Δf increases, the low-frequency data are lost in the one-third octave band spectrum conversion. The lack of data at low frequencies also resulted in differences between the estimated levels below 200 Hz. This would be improved if a logarithmic frequency range was used for the estimation. Overall, the result above 200 Hz did not change significantly, especially at high frequencies. As the frequency resolution is inversely proportional to the computation time, one might consider increasing Δf above 2 kHz, where the difference is less than 2 dB.

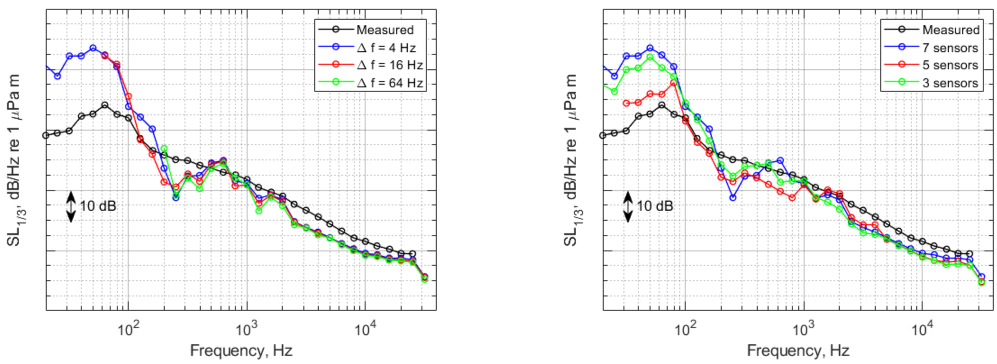

(**a**) (**b**)

Figure 24. Comparison of source levels estimated for other parameters: (**a**) frequency resolution and (**b**) number of sensors.

For the number of sensors, locations "$P1$", "$C0$", "$S1$", "$S2$", and "$F1$" were selected for the five-sensor case and "$C0$", "$S2$", and "$F1$" for the three-sensor case (see Figure 18b). The reason for this is because the propeller rotates counter-clockwise in the propeller plane (looking upstream), and hence, the cavitation is stronger on the starboard side and near the propeller plane. Consequently, the signal-to-noise ratio is expected to be greater around this area. In Figure 24b, good agreement is seen above 1 kHz, where the cavitation noise is dominant. Below this frequency, the result deviates from the reference (seven sensors) by up to 10 dB.

In all cases, except when Δt = 2 s, the high-frequency source level was estimated well, and hence, it can be said that the method has potential to be exploited in underwater radiated noise monitoring. Still, more work needs be done to ensure its robustness and accuracy. This includes optimization of the source region, number of sensors, and data processing.

4. Conclusions

A simple beamforming method for propeller noise monitoring was validated in a model-scale measurement. The method assumed a source grid with virtual monopole sources. An estimated source level was calculated at each source point using noise data measured from the hydrophone array. At each frequency, the beamforming power was calculated for the source grid and the source strength was determined where the beamforming power was at its maximum. For the validation of the method, a commercial ship at model scale was tested in the Large Cavitation Tunnel at the KRISO. In the model-scale measurement, the radiated noise was measured using a hydrophone located in an acoustic window at the bottom. An ITC-1032 transducer was used to measure the transfer function between the source and the receiver. Using the data sheet of the transmitting voltage response, the measured source level was obtained. Good agreement was found between the measured and calculated source levels at frequencies from 2 to 50 kHz.

Full-scale underwater radiated noise and hull pressure measurements were carried out for the application of the estimation method at full scale. The underwater radiated noise was measured using a buoy-type hydrophone array, and the measured result was converted into the source level based on the ISO 17208-1 procedure. For the source-level estimation using on-board sensors, a set of flush-mounted pressure transducers were installed in the hull above the propeller. Comparisons were made between the measured and estimated source levels in one-third octave bands for different operating conditions, showing good agreement above 400 Hz. From the sensitivity analysis, it was revealed that the recording time had little effect on the result at high frequencies, whereas changing the frequency resolution and the number of sensors showed deviations at low frequencies. Nonetheless, the results were consistent in most of the frequency bands.

As the method was only applied to a single ship and the operating conditions were similar, it may need other cases to ensure its robustness and accuracy. In addition, optimization of the source region, number of sensors, and data processing may be studied further.

Author Contributions: Conceptualization, H.J. and H.S.; methodology, J.-H.L. and Y.-H.K.; full-scale measurement, H.S.; model-scale measurement, H J.; data processing and analysis, H.J.; original draft preparation, H.J.; Supervision, H.S.; project administration, H.S. All authors have read and agreed to the published version of the manuscript.

Funding: This work was supported by the Korea Research Institute of Ships and Ocean Engineering (KRISO) under grant number "PES3890" and the Ministry of Trade, Industry, and Energy (MOTIE) under grant number "20012974".

Institutional Review Board Statement: Not applicable.

Informed Consent Statement: Not applicable.

Data Availability Statement: Not applicable.

Acknowledgments: We would like to thank Bong-Chae Kim for providing the URN data measured at full scale.

Conflicts of Interest: The authors declare no conflict of interest.

Abbreviations

The following abbreviations are used in this manuscript:

BPF	Blade-Passing Frequency
IMO	International Maritime Organization
ITTC	International Towing Tank Conference
KIOST	Korea Institute of Ocean Science and Technology
KRISO	Korea Research Institute of Ships and Ocean Engineering
LCT	Large Cavitation Tunnel
MVDR	Minimum-Variation Distortionless Response
PSD	Power Spectral Density
SL	Source Level
SPL	Sound Pressure Level
TVR	Transmitting Voltage Response
URN	Underwater Radiated Noise

References

1. Kaplan, M.B.; Solomon, S. A coming boom in commercial shipping? The potential for rapid growth of noise from commercial ships by 2030. *Mar. Policy* **2016**, *73*, 119–121. [CrossRef]
2. McDonald, M.A.; Hildebr, J.A.; Wiggins, S.M. Increases in deep ocean ambient noise in the Northeast Pacific west of San Nicolas Island, California. *J. Acoust. Soc. Am.* **2006**, *120*, 711–718. [CrossRef]
3. Roll, R.M.; Parks, S.E.; Hunt, K.E.; Castellote, M.; Corkeron, P.J.; Nowacek, D.P.; Wasser, S.K.; Kraus, S.D. Evidence that ship noise increases stress in right whales. *Proc. R. Soc. Biol. Sci.* **2012**, *279*, 2363–2368.

4. Cominelli, S.; Devillers, R.; Yurk, H.; MacGillivray, A.; McWhinnie, L.; Canessa, R. Noise exposure from commercial shipping for the southern resident killer whale population. *Mar. Pollut. Bull.* **2018**, *136*, 177–200. [CrossRef]
5. ISO 17208-1:2016. *Underwater Acoustics–Quantities and Procedures for Description and Measurement of Underwater Sound from Ships–Part 1: Requirements for Precision Measurements in Deep Water Used for Comparison Purposes*; International Standard Organization: Geneva, Switzerland, 2016.
6. Brooker, A.; Humphrey, V. Measurement of radiated underwater noise from a small research vessel in shallow water. *Ocean Eng.* **2016**, *120*, 182–189. [CrossRef]
7. Humphrey, V.; Brooker, A.; Dambra, R.; Firenze, E. Variability of underwater radiated noise measured using two hydrophone arrays. In Proceedings of the OCEANS 2015-Genova, Genoa, Italy, 18–21 May 2015; pp. 1–10.
8. Gassmann, M.; Wiggins, S.M.; Hildebr, J.A. Deep-water measurements of container ship radiated noise signatures and directionality. *J. Acoust. Soc. Am.* **2017**, *142*, 1563–1574. [CrossRef]
9. Johansson, A.T.; Haller J.; Karlsson, R.; Långström, A.; Turesson, M. Full scale measurement of underwater radiated noise from a coastal tanker. In Proceedings of the OCEANS 2015-Genova, Genoa, Italy, 18–21 May 2015; pp. 1–10.
10. McKenna, M.F.; Ross, D.; Wiggins, S.M.; Hildebr, J.A. Underwater radiated noise from modern commercial ships. *J. Acoust. Soc. Am.* **2012**, *131*, 92–103. [CrossRef]
11. Merchant, N.D.; Pirotta, E.; Barton, T.R.; Thompson, P.M. Monitoring ship noise to assess the impact of coastal developments on marine mammals. *Mar. Pollut. Bull.* **2014**, *78*, 85–95. [CrossRef]
12. Garrett, J.K.; Blondel, P.; Godley, B.J.; Pikesley, S.K.; Witt, M.J.; Johanning, L. Long-term underwater sound measurements in the shipping noise indicator bands 63 Hz and 125 Hz from the port of Falmouth Bay, UK. *Mar. Pollut. Bull.* **2016**, *110*, 438–448.
13. The Specialist Committee on Hydrodynamic Noise: Final Report and Recommendations to the 28th ITTC. 2017. Available online: www.ittc.info/media/7837/17-sc-hydrodynamic-noise-compressed.pdf (accessed on 26 January 2021)
14. Seol, H.; Paik, B.-G.; Park, Y.-H.; Kim, K.-Y.; Ahn, J.-W.; Park, C.-S.; Kim, G.-D.; Kim, K.-S. Propeller cavitation noise model test in KRISO large cavitation tunnel and its comparison with full-scale results. In Proceedings of the 4th International Conference on Advanced Model Measurement Technology for the Maritime Industry, Istanbul, Turkey, 28–30 September 2015.
15. Haller J.; Johansson, A.T. Underwater Radiated Noise Measurements on a Chemical Tanker—Comparison Full-Scale and Model-Scale Results. In Proceedings of the 4th International Conference on Advanced Model Measurement Technology for the Maritime Industry, Istanbul, Turkey, 28–30 September 2015.
16. Aktas, B.; Atlar, M.; Turkmen, S.; Shi, W.; Sampson, R.; Korkut, E.; Fitzsimmons, P. Propeller cavitation noise investigations of a research vessel using medium size cavitation tunnel tests and full-scale trials. *Ocean Eng.* **2016**, *120*, 122–135. [CrossRef]
17. Lafeber, F.H.; Bosschers, J. Validation of computational and experimental prediction methods for the underwater radiated noise of a small research vessel. In Proceedings of the 13th International Symposium on PRActical Design of Ships and Other Floating Structures (PRADS' 2016), Copenhagen, Denmark, 4–8 September 2016.
18. Tani, G.; Viviani, M.; Felli, M.; Lafeber, F.H.; Lloyd, T.; Aktas, B.; Atlar, M.; Turkmen, S.; Seol, H.; Hallander J.; et al. Noise measurements of a cavitating propeller in different facilities: Results of the round robin test programme. *Ocean Eng.* **2020**, *213*, 107599. [CrossRef]
19. Bosschers, J. A semi-empirical prediction method for broadband hull-pressure fluctuations and underwater radiated noise by propeller tip vortex cavitation. *J. Mar. Sci. Eng.* **2018**, *6*, 49. [CrossRef]
20. Seol, H.; Suh, J.C.; Lee, S. Development of hybrid method for the prediction of underwater propeller noise. *J. Sound Vib.* **2005**, *288*, 345–360. [CrossRef]
21. Kellet, P.; Turan, O.; Incecik, A. A study of numerical ship underwater noise prediction. *Ocean Eng.* **2013**, *66*, 113–120. [CrossRef]
22. Wu, Q.; Huang, B.; Wang, G.; Cao, S.; Zhu, M. Numerical modelling of unsteady cavitation and induced noise around a marine propeller. *Ocean Eng.* **2018**, *160*, 143–155.
23. Li, D.Q.; Haller J.; Johhanson, T. Predicting underwater radiated noise of a full scale ship with model testing and numerical methods. *Ocean Eng.* **2018**, *161*, 121–135. [CrossRef]
24. Ten, Wolde, T.; De Bruijn, A. A new method for the measurement of the acoustical source strength of cavitating ship propellers. *Int. Shipbuild. Prog.* **1975**, *22.255*, 385–396. [CrossRef]
25. Van Wijngaarden, E. Determination of Propeller Source Strength from Hull-Pressure Measurements. In Proceedings of the Lloyd's List Conference on Noise and Vibration in the Marine Environment, London, UK, 28–29 June 2006.
26. Lee, K.; Lee, J.; Kim, D.; Kim, K.; Seong, W. Propeller sheet cavitation noise source modeling and inversion. *J. Sound Vib.* **2014**, *333*, 1356–1368. [CrossRef]
27. Ahn, B.K.; Go, Y.G.; Rhee, W.; Choi, J.S.; Lee, C.S. Localization of underwater noise sources using TDOA (Time Difference of Arrival) method. *J. Soc. Nav. Archit. Korea* **2011**, *48*, 121–127. [CrossRef]
28. Choo, Y.; Seong, W. Compressive spherical beamforming for localization of incipient tip vortex cavitation. *J. Acoust. Soc. Am.***2016**, *140*, 4085–4090. [CrossRef]
29. Lee, J.H.W. Acoustic localization of incipient cavitation in marine propeller using greedy-type compressive sensing. *Ocean. Eng.* **2020**, *197*, 106894. [CrossRef]
30. Turkmen, S.; Aktas, B.; Atlar, M.; Sasaki, N.; Sampson, R.; Shi, W. On-board measurement techniques to quantify underwater radiated noise level. *Ocean Eng.* **2017**, *130*, 166–175. [CrossRef]

31. Foeth, E.J.; Bosschers, J. Localization and Source-Strength Estimation of Propeller Cavitation Noise Using Hull-Mounted Pressure Transducers. In Proceedings of the 31st Symposium on Naval Hydrodynamics, Monterey, CA, USA, 11–16 September 2016; pp. 11–16.
32. Ahn, J.-W.; Paik, B.-G.; Seol, H.; Kim, G.-D.; Kim, K.-S.; Jung, B.-J.; Choi, S.-J. Comparative study of full-scale propeller cavitation test and LCT model test for MR Tanker. *J. Soc. Nav. Archit. Korea* **2016**, *53*, 180–188.